A Numerical Investigation of Encapsulated Phase Change Materials Melting Process *via* Enthalpy-Porosity Approach

Ghorbany, Mostafa; Esfahlani, Ahad Abedini*+

Energy and Sustainable Development Research Center, Semnan Branch, Islamic Azad University, Semnan, I.R. IRAN

Kargarsharifabad, Hadi

Production and Recycling of Materials and Energy Research Center, Qom Branch, Islamic Azad University, Qom, I.R. IRAN

ABSTRACT: *Today, with the increasing need for energy and the limitation of fossil fuels as depleting and polluting sources of the environment, the need to use more renewable energy sources is felt. The use of PCM materials in buildings, power generation, food industry, and automotive applications is presented .This paper presents the melting process time of a Phase Change Material (PCM) to investigate the impact of various Heat Transfer Fluids (HTFs), using the coupled enthalpy-porosity method and VOF approach. The PCM that is considered is a hydrated salt, Sodium Nitrate ($NaNO_3$) which is encapsulated in a stainless steel infinitely long cylindrical capsule and placed horizontally in a laminar cross flow arrangement with air and Therminol/VP-1 as the HTFs. The Finite-volume-based method has been employed to solve the governing equations for the heat transfer inside and outside the encapsulated PCM. By this technique, the algebraic equations (discretization) are replaced by the governing equations. Then, a set of coupled nonlinear algebraic equations has been solved numerically. The results for the dynamic of the liquid/solid interface at different intervals during the PCM's melting process exhibited that the heat transfer process inside the encapsulated PCM is influenced by HTF types, and PCM melting times are significantly impacted by the flow specifications of HTF on the surface of the capsule.*

KEYWORDS: *Phase change materials; Thermal Analysis; Thermal transfer simulation; Enthalpy-porosity method; Front tracking method.*

INTRODUCTION

Cylindrical phase changes are very important from a theoretical point of view [12] and are important for the development of processes based on the use of latent heat [14]. There is considerable literature in this context, reflecting experimental [10], theoretical [28] and numerical studies of melting [45] and solidification [8]. Phase Change Materials (PCM) are favorable solutions for thermal management systems as they require no power

**To whom correspondence should be addressed.*

+ E-mail: ahad.abedini@gmail.com

1021-9986/2023/7/2275-2285 11/$/6.01

source [22]. In addition, PCMs are utilized for thermal energy storage to extend the lifetime of energy storage systems [23, 38]. In electric vehicles, combining PCM with an active thermal management system is a perfect way of decreasing the power consumption of the cooling system [17, 47]. Nevertheless, modeling and numerical investigation of cylindrical shell polyphase systems, including Phase Change Materials (PCM), and other phase change problems often have obstacles associated with this type of problem [36]. One of the problems in this subject is locating the solid/liquid interface between phases and propagating melt front, in which this causes discontinuities in the quantities at boarder lines [6]. These discontinuities make the modelling and application of boundary conditions difficult on these borders [15]. To calculate the solid/liquid interface, various methods have been conducted that can be classified into two major categories: surface methods [27] and volumetric methods [43]. In the surface method, the interface is represented by specific marker points, and the interpolation method is used to determine the points in between [7]. The advantage of this method is that the location of the interface is always in the specified range and is precisely maintained by propagating it in the flow field [31]. It provides the ability to accurately calculate the curvature and location of interface. One of the limitations of surface methods that occurs during simulation, is that the marker points are either very close together or far apart, consequently decreasing the ability of separation in a fine computational grid [5]. A variety of surface methods can be referred to as forward tracking. In this method, interface is explicitly pursued on a Eulerian grid with non-mass marker particles, and a local velocity with Lagrange approach is used to displace these particles [19]. In this method, when the particles are too far away or close together, the interface is not well defined. [26]. Hence, it is necessary to be removed at specific intervals and added again in each time step [3].

In volumetric methods, it is possible to predict the free surface, or to model the interface between the two phases, and to cover the problems that exist in surface methods, such as discontinuity or surface tension effects, etc. [25]. One of the main volumetric methods is the volume of fluid (VOF), which is also known as volume tracking method [32]. In this method, a scalar function is defined between zero and one called the volume fraction that is employed to identify each of the two phases. One of the great advantages of this method is mass sustainability, which makes this method, superior to other methods. On the other hand, choosing this method is preferred when the boundary strategy changes. Because the VOF method does not require any initial assumptions on the boundary conditions, nor any specific technique for considering these changes at the boundary. Another point is that the VOF method is computationally fast due to deal with the volume fraction only when calculating, which required low space to store data.

In this paper, the methodology is based on VOF for modeling the multiphase media, including solid and molten PCM and predict the interface between two phases. But since this method is not used as a flow-solving algorithm alone, a coupled enthalpy-porosity and VOF method is used simultaneously.

NUMERICAL MODEL

Computational domain and properties

In this investigation, the details of the melting process in an infinitely long cylindrical stainless-steel capsule is explored, for which the diameter is 76.2 mm (3 inches) and the wall thickness is 1.5875 mm (1/16 inch) at a wall temperature of 523 °K. The flow direction is from the capsule's top surface to the bottom, as is depicted in Fig.1. The PCM considered in current study is Sodium nitrate ($NaNO_3$), a hydrated salt which is encapsulated in the cylindrical shaped capsule and placed horizontally in a laminar cross-flow arrangement with air and Therminol/VP1 is the HTFs. Considered Reynolds number for the air and Therminol/VP-1 in laminar flow is 1230 and 29752 respectively, and the initial temperature of HTF is 800 °K. The superficial velocity is measured from 0.01 kg/s to 0.05 kg/s for the HTF's mass flow range.

Phase change of encapsulated PCM is conducted with following assumptions: incompressible molten PCM and HTF flow, two-dimensional geometry, constant physical properties of solid and melted PCM, gravity effects, neglecting natural convection (buoyancy-driven) and volume varieties in the molten PCM. Thermodynamic and physical properties of $NaNO_3$, stainless steel, air, and Therminol/VP-1 as the HTFs are listed in Table 1 and 2.

Governing equations

The external flow of the HTF through the encapsulated PCM, depends on the velocity of the fluid and the type

Table 1: Thermophysical specifications of $NaNO_3$ and stainless steel

	$NaNO_3$		Steel
	Solid	Liquid	-
Density [ρ (kg/m^3)]	2130	1908	8000
Specific heat[C_P (J/kg.K)]	1588	1650	477
Thermal conductivity [k (W/m.K)]	0.05	14.9	0.057
Melting point (K)	581		-
Latent heat of fusion (kJ/kg)	162.5		-

Table 2: Thermophysical properties of the HTF, air and liquid Therminol/VP-1

	Liquid Therminol/VP-1 (698 K)	Air (1 atm, 800 K)
Density [ρ (kg/m^3)]	654	0.4
Specific heat[C_P (J/kg.K)]	2760	1099
Thermal conductivity [k (W/m.K)]	0.07	0.0454
Viscosity (N.s/m2)	1.34×10^{-4}	3.7×10^{-5}
Prandtl number (Pr)	5.3	0.7
Reynolds number (Re)	29752	1230

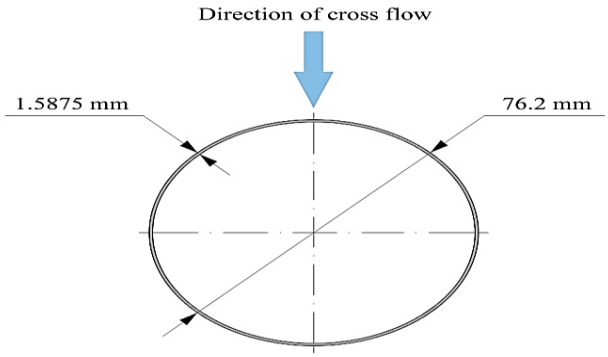

Fig. 1: Cross section of cylindrical shaped capsule

of HTF, which can be laminar or turbulent. Flow regime can be determined by the Reynolds number [18]:

$$Re=\frac{\rho_f U D}{\mu_f} \quad (1)$$

Where ρ_f is density of HTF, U is average velocity, D is diameter of the capsule and μ_f is the fluid viscosity.

Using this definition along with the assumption of Newtonian, incompressible, laminar flow, conduction and convection heat transfer, the governing equations are explained as follows [1]:

Conservation of mass:

$$\frac{\partial \rho}{\partial t}+\frac{\partial(\rho u_i)}{\partial x_i}=0 \quad (2)$$

Conservation of momentum:

$$\frac{\partial u_i}{\partial t}+u_j\frac{\partial u_i}{\partial x_j}=\frac{\mu}{\rho}\frac{\partial^2 u_i}{\partial x_j \partial x_j}-\frac{1}{\rho}\frac{\partial P}{\partial x_i} \quad (3)$$

Where ρ, P, u_i , and u_j denote the density of fluid, the pressure, and velocity vectors in i- and j-directions, respectively.

The equation governing the transient heat transfer in an encapsulated PCM during a thermal storage process (melting) and is given by [11]:

$$\rho_j c_j\left(\frac{\partial T}{\partial t}+u_j\frac{\partial T}{\partial x_j}\right)=\frac{\partial}{\partial x_j}\left(k_j\frac{\partial T}{\partial x_j}\right) \quad (4)$$

Where ρ_j, c_j *and* T_j are the density, the specific heat, and the temperature distribution in each layer, respectively

The subscript *j* for the thin film shell equals to 1, for the liquid phase equals to 2, and for the solid phases of the PCM equals to 3.

The boundary conditions at the outer surface, the interface between the shell and PCM, and the PCM's solid/liquid interface are explained as bellow [13, 39, 44]:

$$-k_1\frac{\partial T_1}{\partial n}=h(T_1-T_f) \quad (5)$$

$$-k_1\frac{\partial T_1}{\partial n}=-k_2\frac{\partial T_2}{\partial n}\ ,\ T_1=T_2 \quad (6)$$

$$-k_2\frac{\partial T_2}{\partial n}=-k_3\frac{\partial T_3}{\partial n}+L\rho_2 V_n\ ,\ T_2=T_3=T_m \quad (7)$$

$$V_n=\frac{\partial s_n}{\partial t} \quad (8)$$

Where *h* and *L*, are the local convective heat transfer coefficient and the PCM's latent heat. Moreover, T_m and T_f represent the PCM's melting temperature and the HTF's temperature, respectively. Also, at the PCM solid/liquid state center for horizontal cylinder [24]is as follows:

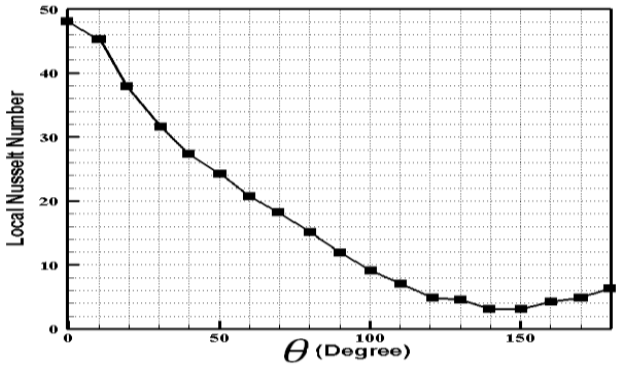

Fig. 2: Local Nusselt number over the cylindrical capsule

$$T_{centroid}=\frac{1}{N}\sum_{1}^{N} T_i \quad (9)$$

Where $T_{centroid}$ and T_i denote the the PCM centroid's temperature and the temperature at nodes around the centroid, respectively. n is the unit normal direction on the surface, V_n is the speed of the interface movement in the normal direction, s_n is the displacement of the liquid/solid interface in the direction normal to the interface and N is the total number of nodes in the angular direction for a horizontally placed cylinder. Initially, the temperature is uniform (T = To) in encapsulated PCM [21].

The temperature of the liquid T_f for a horizontal cylinder is constant, while the convective heat transfer coefficient h, changes with the angular direction around the cylinder. In this context, the local Nusselt number (Nu_φ) is used to calculate the convective heat transfer coefficient [33]:

$$h=\frac{Nu_\varphi.k_f}{D} \quad (10)$$

Where *D* denotes the capsule's outer diameter and k_f represents the HTF thermal conductivity. The coolant's Reynolds number is employed to calculate the local Nusselt number. Fig. 2 exhibits the distribution of the local Nusselt number for the capsule's diameter of 76.2 mm in a cross-flow shape while the employed HTF is air. It was observed that the local Nusselt number on the back of the capsule started to increase for high Reynolds number, but the increase did not have a significant effect on the mean Nusselt number.

Enthalpy-porosity method

The latent heat of melting can be explained by enthalpy method in the energy equation. In this regard, the total amount of heat absorbed during the melting process of each computational model is estimated regarding the temperature of the molten PCM [35]. The ratio of the liquid mass to each cell's mass is considered as the liquid's ratio. This ratio is the baseline for the enthalpy porosity method. The PCM calculation area is divided into three areas: solid, liquid, and pulpy zone (porous area). By determining the temperature distribution, the ratio of liquid , γ, can be calculated [37]. In this way, solid, liquid, and pulpy zones are recognized as γ=0 for liquid region and γ=1 for solid region. Additionally, 0 <γ< 1 indicate the pulpy zone. The enthalpy term is employed to express the energy equation [4]:

$$\frac{\partial}{\partial t}(\rho H)+\frac{\partial}{\partial x_i}(\rho u_i H)=\frac{\partial}{\partial x_i}\left(k\frac{\partial T}{\partial x_i}\right) \quad (11)$$

$$H_s=H_{s\,ref}+\int_{T_{ref}}^{T} C\,dT \quad (12)$$

$$H_L=\gamma L \quad (13)$$

$$H=H_s+H_L \quad (14)$$

The total enthalpy is shown by *H*, where the reference enthalpy is depicted by $H_{s\,ref}$.

Moreover, L, u_i, and T_{ref}, represent the latent heat of fusion, velocity vector, and reference temperature. γ is calculated as [9]:

$$-\begin{bmatrix} \gamma=0 & \text{if} & T<T_{lower} \\ \gamma=1 & \text{if} & T>T_{upper} \\ \gamma=\frac{T-T_{lower}}{T_{upper}-T_{lower}} & \text{if} & T_{lower}<T<T_{upper} \end{bmatrix} \quad (15)$$

Here T_{lower} and T_{upper} denotes the temperatures below the melting temperature and above it. The PCM values of the above-mentioned temperatures specify the mushy region' size. Moreover, the mushy region' size is calculated regarding the heating/cooling rate and the PCM's physical properties.

Volume of Fluid (VOF)

Each cell can be completely specified by one or two phases or a transition zone where the interface line is confined, regarding the volume fraction. In this context, the VOF in the cell is written [2]:

$$\alpha_{i,j}\Delta x.\Delta y\approx\int_i\int_j \alpha_{i,j}\,dx\,dy \quad (16)$$

Where Δx and Δy are grids in x and y spaces, respectively, $\alpha_{i,j}$ is the volume fraction function. To estimate the volume conservation of each cell, the sum of all volume flows must equal the total volume flow. As an example [29]:

$$\sum dV_{i+\frac{1}{2},j}=V_{i+\frac{1}{2},j}=\left(\Delta t\, u_{i+\frac{1}{2},j}\right)A_{i+\frac{1}{2},j} \quad (17)$$

Where *A* denotes the edge vector's area. Equation (17) is used to calculate the control volume regarding the surface velocity on the cell's east side. Therefore, the liquid flowing into adjacent cells can be calculated as follows: [30]:

$$-\alpha_e u_e=u_{i+\frac{1}{2},j}=\frac{V_{i+\frac{1}{2},j}}{\Delta t\times\Delta y} \quad (18)$$

By capturing each fluid's volume fraction (α_q) or calculating one set of momentum equation, two or more immiscible fluids can be simulated using the VOF method. For the volume fraction of phases, the calculation of a continuity equation results in obtaining the interface between the phases [40]:

$$\frac{\partial\alpha_q}{\partial t}+u\frac{\partial\alpha_q}{\partial x_i}=0 \quad (19)$$

When $\alpha_q=0$ the cell doesn't contain q_{th} fluid, when $\alpha_q=1$ the cell contains 100% of q_{th} fluid, and when $0<\alpha_q<1$ the cell contains the interface between the q_{th} fluid and another fluid.

SOLUTION PROCEDURE

The Finite-volume-based method has been employed to solve the governing equations for the heat transfer inside and outside the encapsulated PCM. By this technique, the algebraic equations (discretization) are replaced by the governing equations. Then, set of coupled nonlinear algebraic equations has been solved numerically. The control volume technique includes integrating the governing equations about each control volume; it yields discrete equations that conserve each amount on a control-volume basis [20]. Discretization of the governing equations may be illustrated maximum effortlessly through considering the unsteady conservation equation for transport of a scalar amount φ. this is demonstrated by way of the following equation written in essential form for an arbitrary control volume *V* as follows [42]:

$$\int_V\frac{\partial\rho\varphi}{\partial t}dV+\oint\rho\varphi\vec{u}.d\vec{A}=\oint\Gamma_\varphi\nabla_\varphi.d\vec{A}+\int_V S_\varphi dV \quad (20)$$

Where ρ is the density, $\vec{u}$ is the velocity vector ($=u_i+u_j$ in 2D), $\vec{A}$ is the surface area vector, Γ_φ is diffusion coefficient for φ, ∇_φ is the gradient of φ, S_φ is the source term of φ per unit volume. Equation (20) is carried out to each control volume, or cell, within the computational area. Discretization of equation (20) on an arbitrary control volume or cell yields [34]:

$$-k_1\frac{\partial T_1}{\partial n}=-k_2\frac{\partial T_2}{\partial n}\ ,\ T_1=T_2 \quad (6)$$

$$\frac{\partial\rho\varphi}{\partial t}V+\sum_f^{N_{faces}}\rho_f\varphi_f\vec{u}_f.\overrightarrow{A_f}=\sum_f^{N_{faces}}\Gamma_\varphi\nabla_{\varphi_f}.\overrightarrow{A_f}+S_\varphi V \quad (21)$$

Where N_{face} is the number of faces enclosing cell, φ_f is value of φ convected through face f, $\rho_f\vec{u}_f.\overrightarrow{A_f}$ is mass flux through the face, $\overrightarrow{A_f}$ is area of face, ∇_{φ_f} is the gradient of φ at face *f*, *V* is the cell volume and $\frac{\partial\rho\varphi}{\partial t}V$ is defined in Temporal discretization.

Temporal discretization (Implicit time integration)

The governing equations discretized in both space and time for transient simulations. Spatial discretization for time-dependent equations is similar to steady-state cases, whereas the temporal discretization of transient term $\frac{\partial\rho\varphi}{\partial t}V$, involves the integration of every term in the governing equations over a time step Δt. The integration of the transient terms for the time evolution of a scalar variable φ in a generic expression is straightforward, as shown below [16]:

$$\frac{\partial\varphi}{\partial t}=F(\varphi) \quad (22)$$

Where the *F* function denotes any spatial discretization, backward differences, the first-order accurate temporal discretization is given by:

$$\frac{\varphi^{n+1}-\varphi^n}{\Delta t}=F(\varphi) \quad (23)$$

And the second-order accurate discretization is given by:

$$\frac{3\varphi^{n+1}-4\varphi^n+\varphi^{n-1}}{2\Delta t}=F(\varphi) \quad (24)$$

Where φ is a scalar, n+1 is the value at the next time level, n is the value at the current time level and n-1 is the value at the previous time level.

Here the Implicit time integration method is applied to evaluate $F(\varphi)$ at the future time level as shown below:

$$\frac{\varphi^{n+1}-\varphi^n}{\Delta t}=F(\varphi^{n+1}) \quad (25)$$

Since φ^{n+1} in a given cell is related to φ^{n+1} in neighboring cells through $F(\varphi^{n+1})$, thus:

$$\varphi^{n+1}=\varphi^n+\Delta tF(\varphi^{n+1}) \quad (26)$$

The equation (26) is solved iteratively at each time level before the next time step. The advantage of the fully implicit scheme is that it is unconditionally stable with respect to time step size.

Spatial discretization (second-order upwind scheme)

When higher accuracy is desired, it is accomplished at cell faces through a Taylor series expansion of the cell-centered solution about the cell centroid, using a multidimensional linear reconstruction approach. Hence when second-order upwind scheme is used, the face value φ_f is calculated using the following expression [41]:

$$\varphi_f=\varphi+\nabla\varphi.\Delta\bar{s} \quad (27)$$

Where φ and $\nabla\varphi$ are the cell-centered value and its gradient in the upstream cell, and $\Delta\bar{s}$ is the displacement vector from the upstream cell centroid to the face centroid. Determination of the gradient $\nabla\varphi$ in each cell is required for this equation. The Green-Gauss theorem is used to obtain the gradient of the scalar φ at the cell center c0. following discrete form is written as:

$$(\nabla\varphi)_{c0}=\frac{1}{V}\sum_f^{N_{face}}\bar{\varphi}_f\vec{A}_f \quad (28)$$

In which φ_f is the value of φ at the cellular face centroid. The finite volume method keeps values like temperature, velocity, and pressure by applying a collocated approach. The first-order implicit Euler technique is utilized to calculate the time integration. For the convective term, the volume integral has been changed to surface based on the Green-Gauss theorem. Integration of the central point rule for the surface integral is carried out with second-order accuracy. Using the second-order upwind scheme leads to calculation of the convective term. Also, using the central-differencing scheme results in calculation of the diffusive term. Using the momentum equation as well as the continuity equation, the SIMPLE algorithm is employed to solve the pressure-velocity coupling. In the end, the second-order discretization is carried out in domain to achieve higher accuracies.

RESULTS AND DISCUSSION

This section presents first the convergence test and verification of numerical method. Then, a detailed parametric study of melting process of $NaNO_3$ as the phase change material using air and Therminol/VP-1 at the HTF.

Grid independency

Grid independency test is conducted in order to ensure that the results are not dependent of the grid. Thus, three sizes of grids with the number of nodes: 824, 1764 and 3802 based on the average temperature of PCM at 3600th second for air as the HTF has been created and tested. The results of the enthalpy-porosity method are shown in Fig.3 in which, the temperature of PCM from the grid with 1764 nodes to the next grid with 3802 is not much changed and is almost constant. Thus, it is concluded that the grid with 1764 nodes will also have totally independent results.

Enthalpy-porosity method verification

For validating the proposed scheme, isotherms and location of liquid/solid interface during the melting process obtained by the liquid fraction formulation is compared with the results reported by W. Zhao [46], using the front tracking algorithm.

Fig. 3 shows the enthalpy porosity of an encapsulated PCM with a diameter of 76.2 mm using air as the HTF and the position of the interface at different points during melting as estimated using the front tracking method. Increase, which is shown in Fig. 4, shows the position | of the interface using the enthalpy pore ratio method. The front tracking method records the dynamics of the interface between liquid PCM and solid PCM, for which determines the sharp interface of the melting process at any time. The solid/liquid interface estimated by both methods quickly becomes asymmetric because of the fluctuations in the heat transfer coefficient along with the capsule's outer surface. This comparison shows that the interface positions estimated by the mentioned methods correspond perfectly. The current validation of enthalpy-based technology and grid-independent routines for the phase change process gives confidence to our modelling approach.

Detailed parametric study

Melting process of $NaNO_3$ as PCM, using air as the HTF

Fig. 5 shows the isotherms at different times predicted by the enthalpy porosity method for capsules 76.2 mm in diameter using air as the HTF. Because of local convective heat transfer coefficient distributed on the capsule's surface, the molten PCM has large temperature fluctuations. The value of the heat transfer coefficient of the heat transfer

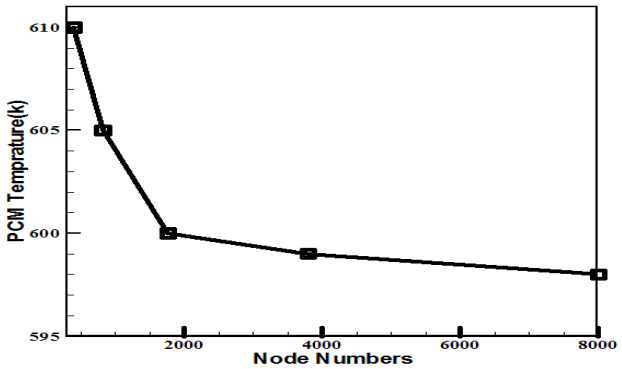

Fig. 3: Results of grid independence of the numerical solution for a 76.2 mm diameter $NaNO_3$ employing air as HTF during melting process(t=3600s)

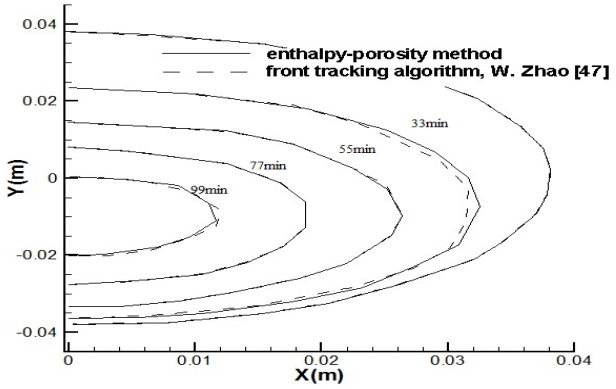

Fig. 4: The liquid/solid interface location during melting process estimated by enthalpy-porosity methodand front tracking algorithm, W. Zhao [46]

coefficient is highest at the top of the cylinder as the HTF flows from top to bottom. Therefore, it can be seen that the temperature at the capsule's top surface is higher than its bottom where isotherms are clear. During the melting process, the heat transfer process within the encapsulated PCM becomes asymmetric due to the effects of gravity, the natural convection of the molten PCM, and the presence, as well as the non-uniform heat transfer coefficient along the capsule's surface. The maximum temperature that reaches the top of the capsule is 594 K, which is higher than the melting temperature of the PCM, $NaNO_3$. Therefore, melting started near the top of the capsule. The temperature of the PCM rises over time. This is because the maximum temperature during the melting process is 606 K in 10 minutes and rises to 693 K in 77 minutes. Here, Fig. 6 (a) depicts the interface formed closed to capsule's top at the beginning of melting. The melt front spreads faster in the capsule's upper area

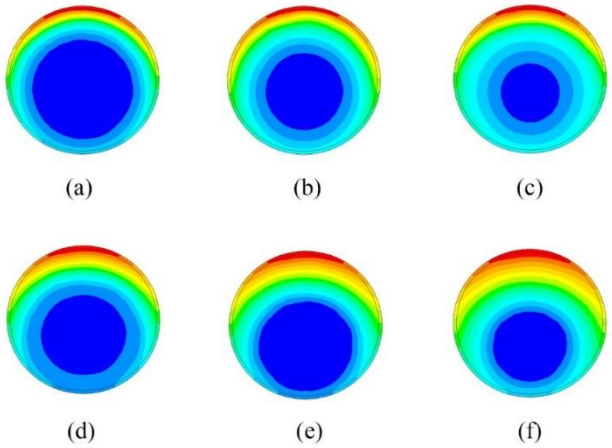

Fig. 5: Contours of static temperature inside the encapsulated $NaNO_3$ at different times during melting at: a) 5 minutes, b) 10 minutes, c) 33 minutes, d) 55 minutes, e) 77 minutes, f) 99 minutes. Air is used as HTF

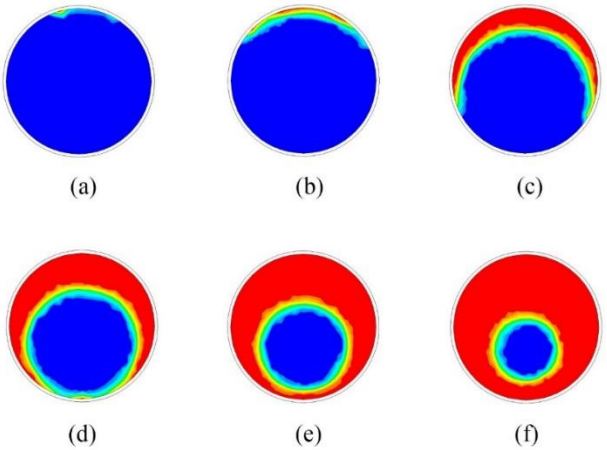

Fig. 6 Contours of liquid fraction inside the encapsulated $NaNO_3$ at different times during melting at: a) 5 minutes, b) 10 minutes, c) 33 minutes, d) 55 minutes, e) 77 minutes, f) 99 minutes. Air is used as HTF

than its lower area. The reason lies behind the fluctuations in the heat transfer coefficient along with the capsule. Fig. 6 (f) demonstrates that in late melting, the solid PCM would be closer to the bottom.

Melting process of $NaNO_3$ as PCM, using Therminol/VP-1 as the HTF

Similarly, the predicted isotherm and interface positions at various points in the melting process for encapsulated PCM with a diameter of 76.2 mm are shown in Figs. 7 and 8 for Therminol/VP-1 as HTF and $NaNO_3$ as PCM. Since the heat transfer coefficient is far higher on

Table 3: Total time of the numerical solution for a 76.2 mm diameter $NaNO_3$ using Air and Therminol/VP-1 as HTFs during melting process

Heat Transfer Fluid (HTF)	Total Melting Time (min)
Air	142.5
Liquid Therminol/VP-1	88

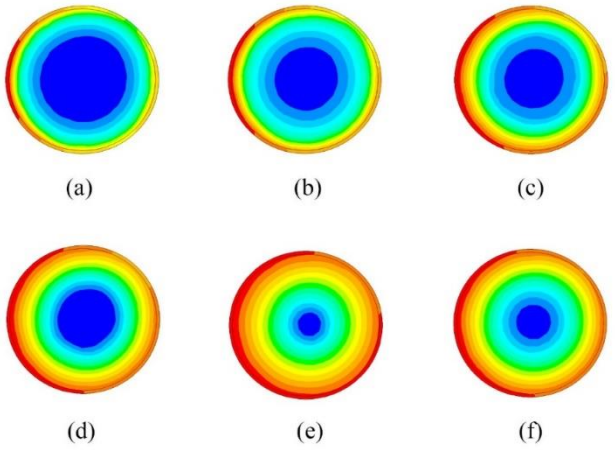

Fig. 7: Contours of static temperature inside the encapsulated $NaNO_3$ at different times during melting at: a) 5 minutes, b) 10 minutes, c) 33 minutes, d) 55 minutes, e) 77 minutes, f) 99 minutes. Therminol/VP-1 is used as HTF

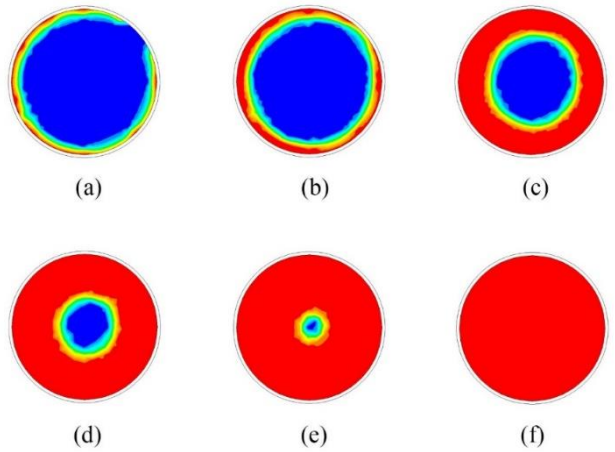

Fig. 8: Contours of liquid fraction inside the encapsulated $NaNO_3$ at different times during melting at: a) 5 minutes, b) 10 minutes, c) 33 minutes, d) 55 minutes, e) 77 minutes, f) 99 minutes. Therminol/VP-1 is used as HTF

the capsule's surface, the phase change is much faster than HTF when comparing to air.

Table 3 depicts the total heat transfer time of the melting process of horizontally placed capsules with a diameter of 76.2 mm employing air and liquid Therminol/VP-1 as HTF. As is obvious, the air's heat transfer time is very longer, while the liquid's HTF highly diminishes the heat transfer time inside the capsule.

CONCLUSIONS

In this study, the melting process time of PCMs was performed with the aim of predicting the effects of different types of HTFs using a method that combines enthalpy porosity and the VOF approach, and then the results were compared with each other. The PCM investigated was sodium nitrate ($NaNO_3$), a hydrated salt encapsulated in stainless steel capsules. Transient 2D heat transfer analysis was carried out employing the enthalpy porosity method. The interfacial dynamics, temperature distribution, and melting process time estimated by enthalpy porosity method were presented. From the analysis, following facts can be concluded:

1. The results of transient heat transfer simulations performed on sodium nitrate as PCM using the enthalpy porosity method are in good agreement with previous experimental and numerical results from the literature.
2. The results exhibit that the heat transfer process of encapsulated PCM is influenced by the type of HTF and the melting time of the PCM is highly impacted by the flow characteristics of the HTF close to the capsule.
3. This study demonstrates that enthalpy-based method is a valuable tool and can be used as a useful and reliable tool in the study of transients in phase change systems.

Received : Jul.14, 2022 ; Accepted : Dec.08, 2022

REFERENCES

[1] Akbarzadeh M., Kalogiannis T., Jaguemont J., Jin L., Behi H., Karimi D., Beheshti H., Van Mierlo J., Berecibar M., A Comparative Study between Air Cooling and Liquid Cooling Thermal Management Systems for a High-Energy Lithium-Ion Battery Module, *Appl. Therm. Eng.*, **198**: 117503 (2021).

[2] Akyurek E.F., Yoladi M., An Experimental Investigation on Melting and Solidification Behavior of Phase Change Material in Cylindrical Latent Heat Storage Units with Minichannel, *J. Energy Storage*, **41**: 102938 (2021).

[3] Al-Hallaj S., Kizilel R., Lateef A., Sabbah R., Farid M., Rob Selman J., "Passive Thermal Management Using Phase Change Material (PCM) for EV and HEV Li-Ion Batteries", *2005 IEEE Veh. Power Propuls. Conf. VPPC*, 376–380 (2005).

[4] Al-Kouz W., Aissa A., Uma S.S., Prakash M., Kolsi L., Moria H., Jamshed W., Younis O., Effect of a Rotating Cylinder on the 3D MHD Mixed Convection in a Phase Change Material Filled Cubic Enclosure, *Sustain. Energy Technol. Assessments*, **51**: 101879 (2022).

[5] Behi H., Behi M., Ghanbarpour A., Karimi D., Azad A., Ghanbarpour M., Behnia M., Enhancement of the Thermal Energy Storage Using Heat-Pipe-Assisted Phase Change Material, *Energies*, **14(19)**: 6176 (2021).

[6] Behi H., Karimi D., Gandoman F.H., Akbarzadeh M., Khaleghi S., Kalogiannis T., Hosen M.S., Jaguemont J., Van Mierlo J., Berecibar M., PCM Assisted Heat Pipe Cooling System for the Thermal Management of an LTO Cell for High-Current Profiles, *Case Stud. Therm. Eng.*, **25**: 100920 (2021).

[7] Behi H., Karimi D., Jaguemont J., Gandoman F.H., Kalogiannis T., Berecibar M., Van Mierlo J., Novel Thermal Management Methods to Improve the Performance of the Li-Ion Batteries in High Discharge Current Applications, *Energy*, **224**: 120165 (2021).

[8] Behi H., Karimi D., Youssef R., Suresh Patil M., Van Mierlo J., Berecibar M., Comprehensive Passive Thermal Management Systems for Electric Vehicles, *Energies*, **14(13)**: 3881 (2021).

[9] Cao Y., Ayed H., Togun H., Alias H., Bouzgarrou S.M., Waehayee M., Marzouki R., Observation the Melting Process of the Phase Change Material inside a Half-Cylindrical with Thermal Non-Equilibrium Porous Media: CFD Simulation, *Case Stud. Therm. Eng.*, **28**: 101496 (2021).

[10] Chen F., Huang R., Wang C., Yu X., Liu H., Wu Q., Qian K., Bhagat R., Air and PCM Cooling for Battery Thermal Management Considering Battery Cycle Life, *Appl. Therm. Eng.*, **173**: 115154 (2020).

[11] Chen H., Abidi A., Hussein A.K., Younis O., Degani M., Heidarshenas B., Investigation of the Use of Extended Surfaces in Paraffin Wax Phase Change Material in Thermal Management of a Cylindrical Lithium-Ion Battery: Applicable in the Aerospace Industry, *J. Energy Storage*, **45**: 103685 (2022).

[12] Chen X., Zhou F., Yang W., Gui Y., Zhang Y., A Hybrid Thermal Management System with Liquid Cooling and Composite Phase Change Materials Containing Various Expanded Graphite Contents for Cylindrical Lithium-Ion Batteries, *Appl. Therm. Eng.*, **200**: 117702 (2022).

[13] Essa F.A., Abdullah A.S., Alawee W.H., Alarjani A., Alqsair U.F., Shanmugan S., Omara Z.M., Younes M.M., Experimental Enhancement of Tubular Solar Still Performance Using Rotating Cylinder, Nanoparticles' Coating, Parabolic Solar Concentrator, and Phase Change Material, *Case Stud. Therm. Eng.*, **29**: 101705 (2022).

[14] Jaguemont J., Karimi D., Van Mierlo J., Investigation of a Passive Thermal Management System for Lithium-Ion Capacitors, *IEEE Trans. Veh. Technol.*, **68(11)**: 10518–10524 (2019).

[15] Javani N., Dincer I., Naterer G.F., Yilbas B.S., Heat Transfer and Thermal Management with PCMs in a Li-Ion Battery Cell for Electric Vehicles, *Int. J. Heat Mass Transf.*, **72**: 690–703 (2014).

[16] Jeong J.H., Hah S., Kim D., Lee J.H., Kim S.M., Thermal Analysis of Cylindrical Heat Sinks Filled with Phase Change Material for High-Power Transient Cooling, *Int. J. Heat Mass Transf.*, **154**: 119725 (2020).

[17] Karimi D., Behi H., Akbarzadeh M., Khaleghi S., Mierlo J. Van, Berecibar M., Optimization of 1D/3D Electro-Thermal Model for Liquid-Cooled Lithium-Ion Capacitor Module in High Power Applications, *Electricity*, **2(4)**: 503–523 (2021).

[18] Karimi D., Behi H., Akbarzadeh M., Mierlo J. Van, Berecibar M., A Novel Air-Cooled Thermal Management Approach towards High-Power Lithium-Ion Capacitor Module for Electric Vehicles, *Energies*, **14(21)**: 7150 (2021).

[19] Karimi D., Behi H., Akbarzadeh M., Mierlo J. Van, Berecibar M., Holistic 1D Electro-Thermal Model Coupled to 3D Thermal Model for Hybrid Passive Cooling System Analysis in Electric Vehicles, *Energies*, **14(18)**: 5924 (2021).

[20] Karimi D., Behi H., Jaguemont J., Sokkeh M.A., Kalogiannis T., Hosen M.S., Berecibar M., Van Mierlo J., Thermal Performance Enhancement of Phase Change Material Using Aluminum-Mesh Grid Foil for Lithium-Capacitor Modules, *J. Energy Storage*, **30** (2020).

[21] Karimi D., Hosen M.S., Behi H., Khaleghi S., Akbarzadeh M., Van Mierlo J., Berecibar M., A Hybrid Thermal Management System for High Power Lithium-Ion Capacitors Combining Heat Pipe with Phase Change Materials, *Heliyon*, **7(8)** : e07773 (2021).

[22] Karimi D., Jaguemont J., Behi H., Berecibar M., Van Den Bossche P., Van Mierlo J., Passive Cooling Based Battery Thermal Management Using Phase Change Materials for Electric Vehicles, *EVS33 Int. Electr. Veh. Symp.*, 1–12 (2020).

[23] Karimi D., Khaleghi S., Behi H., Beheshti H., Hosen M.S., Akbarzadeh M., Van Mierlo J., Berecibar M., Lithium-Ion Capacitor Lifetime Extension through an Optimal Thermal Management System for Smart Grid Applications, *Energies*, **14(10)** (2021).

[24] Kumar A., Agrawal R., An Experimental Investigation of Cylindrical Shaped Thermal Storage Unit Consisting of Phase Change Material Based Helical Coil Heat Exchanger, *J. Energy Storage*, **45**: 103795 (2022).

[25] Lan H., Dutta S., Vahedi N., Neti S., Romero C.E., Oztekin A., Nappa M., Ruales R., Graphite Foam Infiltration with Mixed Chloride Salts as PCM for High-Temperature Latent Heat Storage Applications, *Sol. Energy*, **209**: 505–514 (2020).

[26] Ling Z., Wang F., Fang X., Gao X., Zhang Z., A Hybrid Thermal Management System for Lithium Ion Batteries Combining Phase Change Materials with Forced-Air Cooling, *Appl. Energy*, **148**: 403–409 (2015).

[27] Lv Y., Liu G., Zhang G., Yang X., A Novel Thermal Management Structure Using Serpentine Phase Change Material Coupled with Forced Air Convection for Cylindrical Battery Modules, *J. Power Sources*, **468**: 228398 (2020).

[28] Parhizi M., Jain A., Analytical Modeling and Optimization of Phase Change Thermal Management of a Li-Ion Battery Pack, *Appl. Therm. Eng.*, **148**: 229–237 (2019).

[29] Punniakodi B.M.S., Senthil R., Experimental Study on Melting Enhancement of Phase Change Material in a Vertical Cylindrical Latent Heat Storage Using a Short Concentric Helical Heat Transfer Tube, *J. Energy Storage*, **41**: 102879 (2021).

[30] Raizah Z., Aly A.M., Double-Diffusive Convection of a Rotating Circular Cylinder in a Porous Cavity Suspended by Nano-Encapsulated Phase Change Materials, *Case Stud. Therm. Eng.*, **24**: 100864 (2021).

[31] Rao Z., Wang S., A Review of Power Battery Thermal Energy Management, *Renew. Sustain. Energy Rev.*, **15(9)**: 4554–4571 (2011).

[32] Rudman M., Volume-Tracking Methods for Interfacial Flow Calculations, *Int. J. Numer. Methods Fluids*, **24(7)**: 671–691 (1997).

[33] Selimefendigil F., Öztop H.F., Effects of Flow Separation and Shape Factor of Nanoparticles in Heat Transfer Fluid for Convection Thorough Phase Change Material (PCM) Installed Cylinder for Energy Technology Applications, *J. Energy Storage*, **41**: 102945 (2021).

[34] Selimefendigil F., Öztop H.F., Modeling and Identification of Combined Effects of Pulsating Inlet Temperature and Use of Hybrid Nanofluid on the Forced Convection in Phase Change Material Filled Cylinder, *J. Taiwan Inst. Chem. Eng.*, **119**: 90–107 (2021).

[35] Selimefendigil F., Öztop H.F., Thermal Management and Performance Improvement by Using Coupled Effects of Magnetic Field and Phase Change Material for Hybrid Nanoliquid Convection through a 3D Vented Cylindrical Cavity, *Int. J. Heat Mass Transf.*, **183**: 122233 (2022).

[36] Shafee S.M., Gnanasekaran K., Ravikumar Solomon G., Arshi Banu P.S., Analysis of Heat Transfer Mechanisms During Energy Storage in a Vertical Cylindrical Unit Filled with Nano Enhanced Phase Change Material for Free Cooling Applications, *Mater. Today Proc.*, **22**: 743–750 (2020).

[37] Shaker M.Y., Sultan A.A., El Negiry E.A., Radwan A., Melting and Solidification Characteristics of Cylindrical Encapsulated Phase Change Materials, *J. Energy Storage*, **43**: 103104 (2021).

[38] Sharma A., Trivedi M., Agarwal K., Nirmalkar N., Thermal Energy Storage in a Confined Cylindrical Heat Source Filled with Phase Change Materials, *Int. J. Heat Mass Transf.*, **178**: 121603 (2021).

[39] Sodhi G.S., Muthukumar P., Experimental and Numerical Investigations on the Charging and Discharging Performances of High-Temperature Cylindrical Phase Change Material Encapsulations, *Sol. Energy*, **224**: 411–424 (2021).

[40] Soliman A.S., Zhu S., Xu L., Dong J., Cheng P., Melting Enhancement of Nano-Phase Change Material in Cylindrical Enclosure Using Convex/Concave Dimples: Numerical Simulation with Experimental Validation, *J. Energy Storage*, **44**: 103470 (2021).

[41] Soliman A.S., Zhu S., Xu L., Dong J., Cheng P., Numerical Simulation and Experimental Verification of Constrained Melting of Phase Change Material in Cylindrical Enclosure Subjected to a Constant Heat Flux, *J. Energy Storage*, **35**: 102312 (2021).

[42] Sonker V.K., Chakraborty J.P., Sarkar A., Singh R.K., Solar Distillation Using Three Different Phase Change Materials Stored in a Copper Cylinder, *Energy Reports*, **5**: 1532–1542 (2019).

[43] Sridharan S., Srikanth R., Balaji C., Multi Objective Geometric Optimization of Phase Change Material Based Cylindrical Heat Sinks with Internal Stem and Radial Fins, *Therm. Sci. Eng. Prog.*, **5**: 238–251 (2018).

[44] Tomita S., Celik H., Mobedi M., Thermal Analysis of Solid/Liquid Phase Change in a Cavity with One Wall at Periodic Temperature, *Energies*, **14(18)**: 5957 (2021).

[45] Yang W., Zhou F., Liu Y., Xu S., Chen X., Thermal Performance of Honeycomb-like Battery Thermal Management System with Bionic Liquid Mini-Channel and Phase Change Materials for Cylindrical Lithium-Ion Battery, *Appl. Therm. Eng.*, **188**: 116649 (2021).

[46] Zhao W., "Characterization of Encapsulated Phase Change Materials for Thermal Energy Storage", Lehigh University (2013)

[47] Zhou T., Xiao Y., Huang H., Lin J., Numerical Study on the Cooling Performance of a Novel Passive System: Cylindrical Phase Change Material-Assisted Earth-Air Heat Exchanger, *J. Clean. Prod.*, **245**: 118907 (2020).